Journal of Radiation Research and Applied Sciences 18 (2025) 101700

Contents lists available at ScienceDirect

Journal of Radiation Research and Applied Sciences

journal homepage: www.journals.elsevier.com/journal-of-radiation-research-and-applied-sciences

Exploring the structural, thermal, optical, and γ-ray shielding properties of Bi_2O_3 nanocrystals/polyvinyl acetate/polyvinyl chloride blend

Mohammad W. Marashdeh [a], Aya H. Ahmed [b], Hanan Akhdar [a], K.A. Mahmoud [c,d], Adel M. El Sayed [b,*], A. Abou Elfadl [b]

[a] Department of Physics, College of Sciences, Imam Mohammad Ibn Saud Islamic University (IMSIU), Riyadh, 11623, Saudi Arabia
[b] Department of Physics, Faculty of Science, Fayoum University, El-Fayoum, 63514, Egypt
[c] Ural Federal University, St. Mira, 19, 620002, Yekaterinburg, Russia
[d] R&D Office, Vice Presidency for Scientific Research and Innovation, Imam Abdulrahman Bin Faisal University, P.O. Box 1982, Dammam, 31441, Saudi Arabia

ARTICLE INFO

Keywords:
Thermoplastic blend
Bi_2O_3 nanocrystals
Thermal properties
Gamma-ray protection

ABSTRACT

This study reports the preparation, physical, and γ-ray shielding properties of bismuth oxide nanocrystals/polyvinyl acetate/polyvinyl chloride (Bi_2O_3 NC/PVAc/PVC) films. Fourier transform infrared spectroscopy (FTIR) showed the complexation and hydrogen bonding among the film constituents. X-ray diffraction was employed for the blend structure and filler phase identification. High-resolution transmission and scanning electron microscopy checked the filler and films' morphology, and the Bi_2O_3 NC distribution on the film surface. The optical transmittance, absorption index, and optical conductivity of the films were studied. The blend's optical band gap reduced from 4.2 to 3.8 eV, the Urbach energy increased from 88 to 181 meV, and the refractive index improved from 1.9 to 3.8 (at $\lambda = 630$ nm) with increasing Bi_2O_3 NC. The films were subjected to thermal analyses up to 600 °C to investigate the thermal stability and transition temperatures. The gamma-ray protection capacity for the synthesized composites was examined using the Monte Carlo simulation techniques over the low energy range, which extends from 15 keV to 356 keV. The role of the enrichment of Bi_2O_3 NC on the protection properties of the synthesized composites was deeply examined. The enrichment of Bi_2O_3 NC concentration shows an enhancement in the linear attenuation coefficient and radiation protection efficiency of fabricated films, while the lead equivalent thickness for the composites reduced.

1. Introduction

The widespread utilization of ultraviolet (UV), X-ray, and gamma (γ)-rays in medical and industrial sectors forces researchers to develop new materials that efficiently shield these radiations (Almuqrin et al., 2024). Many materials have been used as shields: concrete, alloys, ceramics, rocks, glasses, and polymer-based nanocomposites, which are composed of a polymer or blend (two or more polymers) filled with a nano-sized inorganic material, *i.e.*, metal, metal oxide, etc. This class exhibits interesting features such as ease of manufacture and processing, transparency, flexibility, eco-friendliness, low cost, lightweight, and low maintenance (Alyousef et al., 2023; Hamisu et al., 2024; Kassim et al., 2025; Yazdani-Darki et al., 2025). In addition, blending the polymers is a direct approach to harnessing the advantages of each polymer in one material useful for a broader range of applications (Menon et al., 2022; Wu et al., 2025).

The nano-sized fillers are preferred to microparticles, as the distance between the atoms is so small at the nanoscale, resulting in a higher probability of interaction between the atoms and incident photons (Almuqrin et al., 2024). Since the nano-fillers have a high surface-to-volume ratio, they can alter the molecular structures, strength, and stiffness of the polymers. They can also increase the surface area, gas permeability, heat resistance, and γ-ray interaction frequency of the film, which will increase the radiation absorption efficiency (Kassim et al., 2025). The photoelectric absorption probability is proportional to (the atomic number (Z)/photon energy)^3 (Messele et al., 2025). Therefore, the higher the Z value, density (ρ), and thermal properties of the nano-fillers, the better the performance of the shielding ability of the material (absorb or attenuate most of the incoming photons) (Hamisu et al., 2024). Bi_2O_3 ($\rho = 8.9$ g/cm^3) is very appealing owing to its affordability, less toxicity compared to other heavy metals (Pb has environmental and toxic effects), high stability (high melting

* Corresponding author.
E-mail address: ams06@fayoum.edu.eg (A.M. El Sayed).

https://doi.org/10.1016/j.jrras.2025.101700
Received 12 May 2025; Received in revised form 5 June 2025; Accepted 9 June 2025

and boiling points of 817 and 1980 °C (Echeweozo et al., 2025)), ease of synthesis, and $Z_{Bi} = 83$ is very suitable for photon absorption at lower energies (Alyousef et al., 2023; Koyuncu et al., 2024).

Koyuncu et al. (Koyuncu et al., 2024) developed a coating layer (60 wt% Bi_2O_3/40 wt% waterborne polyurethane) wearable (cotton) woven fabrics with enhanced X-ray shielding performance and textile properties. Gholamzadeh and Mehrjardi (Gholamzadeh & Mehrjardi, 2024) studied the X-ray shielding performance of Bi_2O_3/polyvinyl alcohol (PVA)/polyester fabric prepared by electrospinning. Kamaruddin et al. (Kamaruddin et al., 2024) studied the influence of Bi_2O_3(5–20 %)/WO_3(10 %) on the X-ray (16.61–25.27 keV) attenuation performance of the electrospun PVA/Al collector. Water-insoluble polymers, such as polyvinyl chloride (PVC), polystyrene (PS), polyvinyl acetate (PVAc), polyvinylidene fluoride (PVDF), polymethyl methacrylate (PMMA), high-density polyethylene (HDPE), polydimethylsiloxane (PDSM), polychloroprene (PCP), and polylactic acid (PLA) are the most practical choice for developing radiation shielding materials. Almuqrin et al. (Almuqrin et al., 2024) found that using a mix of micro and nano-sized Bi_2O_3 is preferred to using micro or nano-size particles to improve the shielding aspect and the γ-rays attenuation properties of PDSM. Alyousef et al. (Alyousef et al., 2023) reported that 10 % Bi_2O_3/PMMA exhibits interesting shielding properties comparable to those of concrete and gypsum. Kassim et al. (Kassim et al., 2025) evaluated the efficiency of Bi_2O_3/Ti_6Al_4V/glycidyl methacrylate in low-energy (< 200 keV) γ-rays attenuation. Messele et al. (Messele et al., 2025) loaded micro- and NPs of $BaSO_4$ and Bi_2O_3 as additives into polychloroprene (PCP) for obtaining Pb-free X-ray protectives. $BaSO_4$ enhanced the shielding performance at 80 kV and Bi_2O_3 enhanced the protective properties at higher tube voltage (120 and 135 kV). Echeweozo et al. (Echeweozo et al., 2025) prepared Bi_2O_3/PMMA composites by ball milling and heat treatment at 200 °C to design the medical apron for X/γ-ray shielding. Yassene et al. (Yassene et al., 2024) developed γ-ray and neutron shielding utilizing HDPE loaded with BaO nanowires/Bi_2O_3 nanorods/boric acid. Besides the improved thermal and mechanical properties, they reported that 1.5 wt% of both Bi_2O_3 and BaO improved the γ-rays attenuation. Özdemir et al. (Özdemir et al., 2024) utilized Bi_2O_3 and expanded graphite/micro/nano-sized CuO inside the PVDF (0.2–0.24 mm thickness) for RF and electromagnetic interference shielding (EIS) in the 8–12 GHz range.

Among the thermoplastic polymers, PVAc is a nontoxic, colorless, thermoplastic, rubbery, degradable polymer, and a very strong/water-based adhesive for concrete, wood, textile, glass-reinforced plastics, ceramic porous materials, packaging industries, furniture, EIS, and humidity sensing materials (Menon et al., 2022; Sameela et al., 2023; Tan et al., 2025; Yu et al., 2025). The active ester group on the PVAc's skeleton frame is a source of interaction with nano-fillers via H bonding (Sameela et al., 2023). Tan et al. (Tan et al., 2025) fabricated copper abietate/PVAc films for enhanced humidity-sensing performance of monitoring systems for herbal medicine. Zhang et al. (Zhang et al., 2022) studied the PVAc's mechanical properties under the impact of both carbon dots 2.5–8.5 nm in size, and carbon black. They observed that the viscosity, reputation relaxation time, tensile stress, and elongation at break are very sensitive to the filler size. However, owing to the poor performance of PVAc at high temperatures and poor moisture and humidity resistance, PVAc was blended with other thermoplastic polymers (Sameela et al., 2023). Wu et al. (Wu et al., 2025) used PVAc-modified cellulose nanocrystals (CNC) as nanofillers to enhance the mechanical properties of PLA, maintaining its degradability and biocompatibility. They found that PVAc inhibits the CNC thermal decomposition, and enhances the segmental mobility of PLA. PVAc in the PVAc/PMMA/GO composite was used to adjust the GO distribution and restrict their aggregation (Yu et al., 2025). On the other hand, PVC is one of the most popular matrices for hosting nanofillers for shielding purposes owe to its good elasticity, mechanical strength, thermal stability, easy preparation, low cost, safety, and transparency (Yazdani-Darki et al., 2025). Nunez-Briones et al. (Nunez-Briones et al., 2024) prepared Bi_2O_3 NPs and nanowires by different techniques and incorporated them inside PVC for shielding against X-ray radiation, where the nanowires revealed the best performance due to their good distribution.

Lead aprons, thyroid collars, gloves, and goggles are all examples of equipment that falls under the category of personal protective equipment (PPE) for X-ray and gamma-ray protection. These products aim to shield vital organs such as the thyroid from the damaging effects of radiation and provide suitable levels of protection against it. These PPEs frequently utilize lead-based materials with high effectiveness in reducing radiation effects (Lakhwani et al., 2019) Compared to PbO, which is utilized in personal protective equipment (PPE), the Bi_2O_3 molecule has a number of advantages, including a greater effective atomic number (Z_{eff}), greater interaction cross-section for photons, a lower toxicity level, and a higher density. Consequently, Bi_2O_3 can be utilized as a substitute for lead in order to develop high-efficiency PPES, which is utilized in the nuclear medicine applications at hospitals (Nancy D'Souza et al., 2020).

The literature survey reveals that radiation shields based on the thermoplastic PVAc/PVC blend modified with Bi_2O_3 nanocrystals (NC) have not yet been reported. In addition, the mixed morphology of NC ((nanorods, nanoparticles, and sheets) could provide various ways for interaction with the polymeric matrix.

The novelty of the current work is to develop a new Bi_2O_3 NC/PVAc/PVC nanocomposite by simple sol-gel and casting techniques. The structure, thermal, and optical properties of the synthesized films were investigated. Furthermore, the evaluation of the influence of the enrichment of Bi_2O_3 NC concentrations within the PVAc/PVC material on the γ-ray protection characteristics was conducted across the low energy interval that was bordered by 15 keV and 356 keV.

2. Experimental procedures

2.1. Chemicals, method, and characterization

Bismuth subcarbonate powder [$(BiO)_2CO_3$, ~510 g/mol, PubChem, USA] was used to prepare Bi_2O_3 nanocrystals. 0.5 M solution was obtained by dissolving 25.5 g of [$(BiO)_2CO_3$ in 100 mL of pure water using a bar magnet for about 1.0 h in a beaker. 6.33 g of oxalic acid was stirring until dissolving in 25 mL of pure water and added to the first solution. The mixed solution was stirred for another 1.0 h and then put to dry in a furnace at 100 °C for 3.0 h to remove the excess water. The obtained white gel was aged for 12 h at room temperature (RT) and then calcined at 450 °C for 2.0 h. The final powder was saved in a zipper bag to prevent moisture.

The PVAc/PVC blend film was prepared by dissolving 0.65 g of PVAc [from Alpha Chemika, Mumbai, India] in 35 mL of tetrahydrofuran (THF) [Aldrich, Germany] in a beaker (tightly closed) for 0.5 h at 60 °C. 0.35 g of PVC [from Essex (Ltd., UK)] in THF (20 mL) for 0.5 h at RT. The PVAc and PVC solutions were mixed and stirred for another 0.5 h. The mixed solution was poured into a Petri dish and left to dry (THF evaporation) for 1 day at RT. Bi_2O_3 NC/PVAc/PVC films were prepared following the same steps. About 0.01, 0.03, and 0.06 g of Bi_2O_3 NC were ultrasonicated in 10 mL of THF and added to the mixed solution, the nanocomposite solution was ultrasonicated and stirred 10 min for each, to ensure the uniform filler distribution. Photo images for the obtained films are shown in Fig. S1 (the supplementary materials file).

The interaction, bonding, and complexation among PVAc's, PVC's functional groups, and Bi_2O_3 NC were identified through recording the transmittance (Fourier transform infrared, (FT-IR)) spectra (in the 400–4000 cm^{-1} wavenumber range) employing the spectrophotometer of a Bruker-vertex70, with a diamond attenuated total reflection (ATR) unit. The structure (amorphous/crystalline) of the Bi_2O_3 NC/PVAc/PVC films was studied using the RIGAKU Smart Lab. The device operated at 30 mA and 40 kV and scanned the samples with 0.02° step in the 10–80° 2θ range, where the wavelength (λ) of the used Cu (K_α) = 1.542 nm. The

Bi_2O_3 NC morphology was studied employing a JEM, 2100, Jeol transmission electron microscopy of high-resolution at 200 kV using a carbon-coated copper grid to load the powder. The cross-sectional and surface morphology of the films were investigated using the Inspect S, FEI scanning electron microscopy (The Netherlands). The UV-vis-NIR spectra (transmittance and absorption) were recorded in the 200–1500 nm λ range at 2 nm step using JASCO 630 spectrophotometer. In addition, the reflectance from the film was detected by employing the integrating sphere. The thermal analyses (weight loss vs temperature and transition temperatures) were explored by the PerkinElmer-STA-6000 in a 30–600 °C/N_2 atmosphere.

2.2. Radiation shielding

Using the MCNP-5 code (Monte Carlo N-Particle transport) (X-5 Monte Carlo Team, 2003), the shielding effectiveness of the synthesized Bi_2O_3 NC/PVAc/PVC films was examined over a range of γ-ray energies from 15 to 356 keV. In the simulation process, determining the average track length (ATL, cm) of γ-rays across the synthesized Bi_2O_3 NC/PVAc/PVC sheets was the most important stage. In the input file, the photon tally card was chosen to be F4 in order to estimate the previously specified ATL of γ-ray across the cell containing the Bi_2O_3 NC/PVAc/PVC sheets. Additionally, the input file includes the necessary data regarding the materials, cutoff, tally, cell, surface, and source (SDEF) cards. The interaction cross-sections (σ) required to run the evaluation procedure were taken from the nuclear database ENDF/B-VI.8, and they were modified in the input file that was created. The geometry utilized for the simulation process is described in the input file; it includes a sizable, evacuated lead cylinder that shields the detector from ambient background radiation. The height and diameter of the aforementioned lead cylinder are 40 cm and 35 cm, respectively. The radioactive source has a position of POS (0 0 0) within the constructed cylinder of lead. Through the +Z direction AXS (0 0 1), the monoenergetic photons (PAR: 2) were released. A lead collimator of 7 cm in height and 5 cm in diameter, with a vertical narrow slit in the middle, was used to collimate these photons. Perpendicularly released photons can reach the cylindrically shaped Bi_2O_3 NC/PVAc/PVC film. In order to directed the transmitted photons from samples to the detector, a second collimator was used to collimate. Photon emissions were stopped by the cutoff card's NPS after 10^8 historical. The simulation is finished, and a new output file is automatically created with the relative error in the ATL simulation process, which reach ±0.2 %.

Using the simulated values of ATL (cm), Eq. (1) was utilized to estimate the linear attenuation coefficient (LAC, cm^{-1}), which is considered the primary radiation shielding parameter. The I_o and I_t represent the photons intensities before and after interaction with the synthesized Bi_2O_3 NC/PVAc/PVC films. Furthermore, x (cm) indicates the thickness of synthesized Bi_2O_3 NC/PVAc/PVC films.

$$\mu = \left(\frac{1}{x}\right) ln\left(\frac{I_0}{I_t}\right) \tag{1}$$

Half-value thickness (HVL, cm) represents the thickness of Bi_2O_3 NC/PVAc/PVC film which can stop 50 % of the incident Io photons. It can be determined according to Eq. (2).

$$HVL\ (cm) = \frac{\ln(2)}{LAC} \tag{2}$$

The thickness of the synthesized Bi_2O_3 NC/PVAc/PVC films which have the same shielding performance (LET) as 0.05 cm of pure lead which used in the medical protection applications was calculated according to Eq. (3).

$$LET(cm) = \frac{\left(\ln\left(\frac{I_o}{I_t}\right)\right)_{Lead}}{\left(\ln\left(\frac{I_o}{I_t}\right)\right)_{composite}} \tag{3}$$

3. Results and discussion

3.1. Structural and morphological features of the samples

Fig. 1(a) displays the FTIR spectra of Bi_2O_3 NC/PVAc/PVC. In the high wavenumbers region (2000–4000 cm^{-1}) only four bands exist in the spectrum of the PVAc/PVC blend. The band at 2351 cm^{-1}, arises from the stretching of CO_2 adsorbed from the air (Abou Elfadl et al., 2022). The enhanced intensity of this band in the nanocomposite films indicates that Bi_2O_3 NC increases the ability of the blend to interact with the surroundings. The three bands at 2862, 2908, and 2970 cm^{-1} arise from the vibrations of CH_2 (symmetric), sp^3 C–H bond, and CH_2 (asymmetric), respectively (Abdelghany et al., 2019; Khan et al., 2020). The strength of these vibrations is significantly reduced upon loading Bi_2O_3 NC. The hydrogen bonding between Bi_2O_3 NC and the blend functional groups restricts their vibrations and reduces the number of available groups.

In the 400–2000 cm^{-1} wavenumber range there are various bands. The two bands at 1720 and 1425 cm^{-1} characterize the PVAc and PVC, respectively, where the first band arises from the PVAc's carbonyl group (C=O) vibration (Dogan et al., 2021) and the second band indicates the CH_2–Cl's angular deformation (El Sayed et al., 2022). Additionally, the CH–Cl angular deformations (out of plane) and the stretching vibration of the C–Cl bond of PVC appears at 1255 cm^{-1}, and at 607 and 691 cm^{-1}, respectively (Elashwai et al., 2008). The weakness of these bands with increasing Bi_2O_3 NC content in the blend indicates the efficient composite formation in these films (Tan et al., 2025). The other bands at 1330, 1062, and 957 cm^{-1} correspond to CH_2 deformation, and the stretching vibration of C–C, r(CH_3) vibrations of PVAc (Abdelghany et al., 2019). Moreover, the FTIR spectrum of the PVAc/PVC blend loaded with 1.0 wt% Bi_2O_3 NC displays two additional peaks at 434 and 511 cm^{-1}. The first one shifted to 445 cm^{-1} with increasing Bi_2O_3 NC content, confirming the physical interaction between Bi and O atoms of the filler with blend functional groups. Additionally, a new peak is seen at 847 cm^{-1} in the spectrum of 6.0 wt% Bi_2O_3 NC/PVAc/PVC film. These peaks belong to Bi–O and Bi–O–Bi vibrations, confirming the presence of Bi_2O_3 in the blend. Similarly, Messele et al. (Messele et al., 2025) detected a wide peak in the 400–700 cm^{-1} wavenumbers due to Bi–O–Bi vibration.

Fig. 1(b) depicts XRD charts of blend and nanocomposite films. A halo peak extends from 15° to 28° on the 2θ scale, indicating the amorphous structure of the PVAc/PVC blend. This is an expected result, where it is known that PVAc and PVC are amorphous polymers with a broad hump in the region of 2θ = 12–32° and 13–34°, respectively (El Sayed & Morsi, 2013; Menon et al., 2022). Incorporating Bi_2O_3 NC resulted in a reduction in the hump height. The main XRD peaks at 2θ (*hkl*) = 24.43° ($10\bar{2}$), 25.62° (002), 26.80 ($11\bar{2}$), 27.27° ($12\bar{1}$), 27.86° (012), 32.89° ($12\bar{2}$), and 33.09° (20 $\bar{2}$). This pattern confirms the formation of the Bismite (α-Bi_2O_3) phase of the monoclinic structure and *P21/c* space group (DB and JCPDS cards numbers: 9012546 and 76–1730, respectively. A full XRD spectrum of Bi_2O_3 NC is provided in Fig. S2 (the supplementary materials file). These peaks exhibit growing intensities with increasing Bi_2O_3 NC content. A similar pattern was reported for Bi_2O_3 NPs prepared by hydrothermal process (Gholamzadeh & Mehrjardi, 2024). The inset of this figure illustrates that the peaks of Bi_2O_3 NC in the 1.0 wt% Bi_2O_3 NC shifted to the left by less than 0.15° with increasing filler content to 6.0 wt%. Similarly, the broad hump of the unsaturated polyester resin became barely visible and the Bi_2O_3's XRD peak was left-shifted with increasing Bi_2O_3 content (Ghule et al., 2024). These results support the FTIR results and confirm the complexation between Bi_2O_3 NC and the blend.

Fig. 2(a) shows the HR-TEM investigation of the sol-gel-obtained Bi_2O_3. The image indicates that the sample consists of components with different morphologies (nanocrystals): spherical particles with diameters in the range of 41–100 nm, rods having widths in the range of

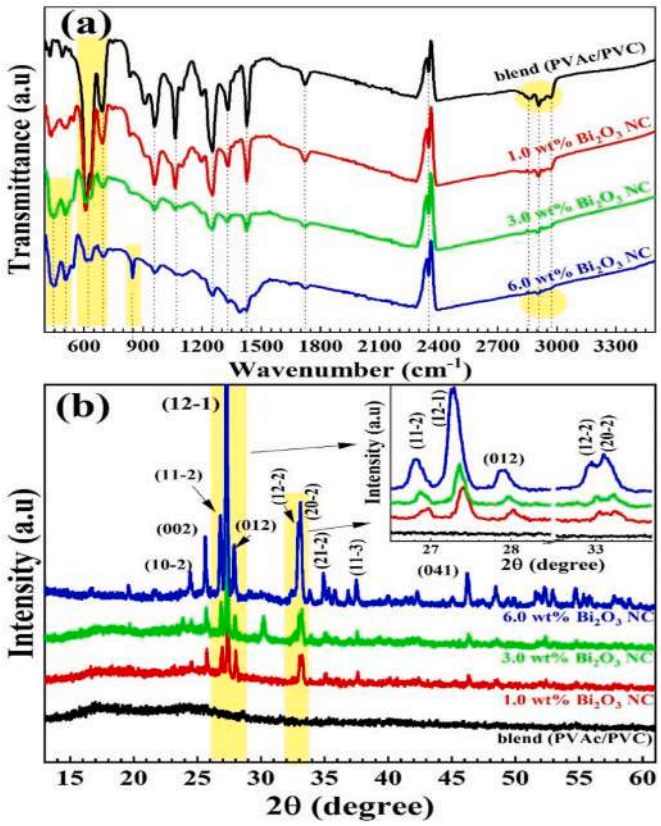

Fig. 1. (a, b): FTIR spectra and XRD patterns of neat and Bi_2O_3 NC-doped PVAc/PVC films.

26–50 nm, and sheets. Similarly, a coprecipitation route was employed to prepare Bi_2O_3 NPs with grain sizes of 51–71 nm (Ahamed et al., 2021). A sonochemical approach was adopted to obtain Bi_2O_3 microrods of a diameter of 0.45 μm and lengths of 9.72–2.48 μm (Kavgacı & Eskalen, 2023). Fig. 2(b) shows a single Bi_2O_3 particle's selected area electron diffraction. The white spots form circular paths or a diffraction pattern similar to the XRD pattern. These results indicate the good crystallinity of Bi_2O_3 NC and the consistency between XRD and TEM investigations.

Fig. 2(c, d) shows surface images of 1.0 and 6.0 wt% Bi_2O_3 NC/PVAc/PVC near the edges (the fracture cross-section) of the films. The film's surface seems to have a sponge-like morphology. The films have almost the same thickness (123–128 μm). Fig. 2(e, f) displays a closer look at the top surface of the films. The films have a porous surface structure, and PVAc (65 %) and PVC (35 %) polymers are shown to be miscible. This is consistent with the study carried out by Abdelghany et al. (X-5 Monte Carlo Team, 2003), where PVC/PVAc ratios of 80/20, 50/50, 30/70, 20/90, and 10/90 showed good miscibility. Bi_2O_3 NC is evenly distributed on the films with some points of agglomeration. This takes place when the particles get closer together due to the high surface energy of the nano-sized materials.

3.2. Optical properties of the Bi_2O_3 NC/PVAc/PVC films

The transmittance (UV-vis-NIR) spectra of the blend (PVAc/PVC) and nanocomposite films are shown in Fig. 3(a). The neat blend shows about 66 % transmittance at $\lambda \geq 300$ nm. This value decreased with increasing Bi_2O_3 NC content, where at 1.0 wt% Bi_2O_3 NC, the transmittance is in the range of 48–58 % and decreased to 21–35 % at 6.0 wt % Bi_2O_3 NC. The uniform Bi_2O_3 NC distribution seen from SEM images (Fig. 2(e and f)) suggests that these fillers absorb and scatter the incoming photons at the expense of the transmitted portion. A similar finding was reported for $LaFeO_3$- and $PbTiO_3$-loaded PVAc/PVC (Alruwaili & El Sayed, 2024a). This lost photonic energy via absorbing and scattering can be accounted through the absorption index k, where $k = 2.303 \times \text{absorption} \times \lambda/(4 \times 3.14 \times \text{film thickness})$ (Abou Elfadl et al., 2022). Fig. 3(b) shows that the blend film has low k values ($\leq 2 \times 10^{-4}$) in most of the studied λ range. The nanocomposite films show improved k values which increase linearly with λ and approach the maximum (4–7.5) $\times 10^{-4}$ at $\lambda = 1300$ nm. At lower λ, the spectra contain two bands with improved intensity as the Bi_2O_3 NC content increases. The band at 208 nm (denotes the presence of C–Cl bonds) and the band at 278 nm (denotes to C=O bonds) confirm the presence of both PVC and PVAc, supporting the FTIR results.

The indirect band gap (E_g) can be determined considering Tuac's relation (Abdelghany et al., 2019; Abou Elfadl et al., 2022): $(\alpha \times h\upsilon)^{0.5} = A\left(h\upsilon - E_g\right)$, where A is a constant has values in the range of 10^{-8}–10^{-7} m^{-1} (Alhazime et al., 2019), α is the absorption coefficient, and $h\upsilon$ is the photonic energy. Fig. 3(c) shows the $(\alpha \times h\upsilon)^{0.5}$ vs. $h\upsilon$, where extending the linear portions of these curves to meet the x-axis (zero absorption) gives the E_g values. The blend's E_g value is 4.2 eV, reduced to 4.1, 4.0, and 3.8 eV upon incorporating 1.0, 3.0, and 6.0 wt% Bi_2O_3 NC, respectively. Elashmawi et al. (Elashwai et al., 2008) reported E_g value of 5.0 eV for PVAc shrank to 4.21 eV by blending with 75 % polystyrene. Another research group found that 7.0 wt% Boehmite NPs reduced the E_g of PVAc from 3.757 to 3.585 eV (Sameela et al., 2023). Similar findings were reported for the PVAc (5 %)/PVC (50 %) blend where its E_g was reduced from 4.18 eV to 4.1, 3.95, and 3.7 eV when loaded with 1.0 wt% MgO, 1.0 wt% PbO, and 4.0 wt% $Pb_{0.75}Mg_{0.25}O$ NPs, respectively (Abou Elfadl et al., 2022; Alanazi & El Sayed, 2023). This reduction in E_g values arises from the uniform distribution (seen in Fig. 2(c and d)) of the Bi_2O_3 NC which can form connected pathways, facilitating the charge carriers, motion inside the matrix. In addition, these fillers create disorder and new localized states having widths (Urbach energy E_U) depend on α according to $\alpha = C \times \text{Exp}\left(\frac{h\upsilon - A}{E_U}\right)$ (Abou Elfadl et al., 2022), where C and A are constants. This relation can be written as $\text{Ln}\,\alpha = \text{Ln}\,C + \frac{h\upsilon - A}{E_U}$, from which the $E_U = (\Delta \text{Ln}\,\alpha/\Delta h\upsilon)^{-1}$. Fig. 3(d) shows the plots of Ln α vs. $h\upsilon$, where $E_U = (\text{slope})^{-1}$. The determined E_U values (meV) = 88, 124, 118, and 181 for the blend, 1.0, 3.0, and 6.0 wt% Bi_2O_3 NC/blend films, respectively. The E_U values are inversely proportional to E_g values. A similar notice was reported for other polymer composites (Alhazime et al., 2019). The E_U values indicate that Bi_2O_3 NC increase the disorder in the materials, and feasible the ion diffusion and the charge carriers from the valence to conduction bands of the blend.

The index of refraction (n-index) is a very interesting optical parameter for films to be used for coatings and optoelectronic devices. Because the k values are very small ($\sim 10^{-4}$), the n-index can be calculated using the reflectance (R) spectra: $n = \left(1 + R^{\frac{1}{2}}\right)/\left(1 - R^{\frac{1}{2}}\right)$ (Alanazi & El Sayed, 2023). Fig. 4(a) and its inset depict the n-index distribution and R spectra of the films. PVAc/PVC has an almost constant n-index value of about 1.9. Loading 1.0, 3.0, and 6.0 wt% Bi_2O_3 NC turned the R spectra and n-index behaviors to take a bell-shaped form with maximum values of about 2.30, 2.95, and 3.8, respectively, at $\lambda = 630$ nm. A similar behavior was noticed in the n-index spectra of the PVA/PVP blend loaded with 0.5 – 1.5 wt% Bi_2O_3 NPs (Alruwaili & El Sayed, 2024b). Loading the PVAc/PVC blend with highly dense fillers (8.9 g/cm^3) is expected to increase the scattering ability and enhance the films' packing density, making the host highly reflective for the incident light (El Sayed & Mohamed, 2018). The optical conductivity $\sigma_{UV/vis} = \frac{nc\alpha}{12.56}$ (Alanazi & El Sayed, 2023) of the films, where c is the light velocity, was determined and is shown in Fig. 4(b). The $\sigma_{UV/vis}$ is nearly zero at approximately $h\upsilon \leq 4.1$ eV. Only the UV photons can excite the electrons in the films to higher energy levels to take part in the conduction process. Increasing Bi_2O_3 NC level increased the $\sigma_{UV/vis}$, where the

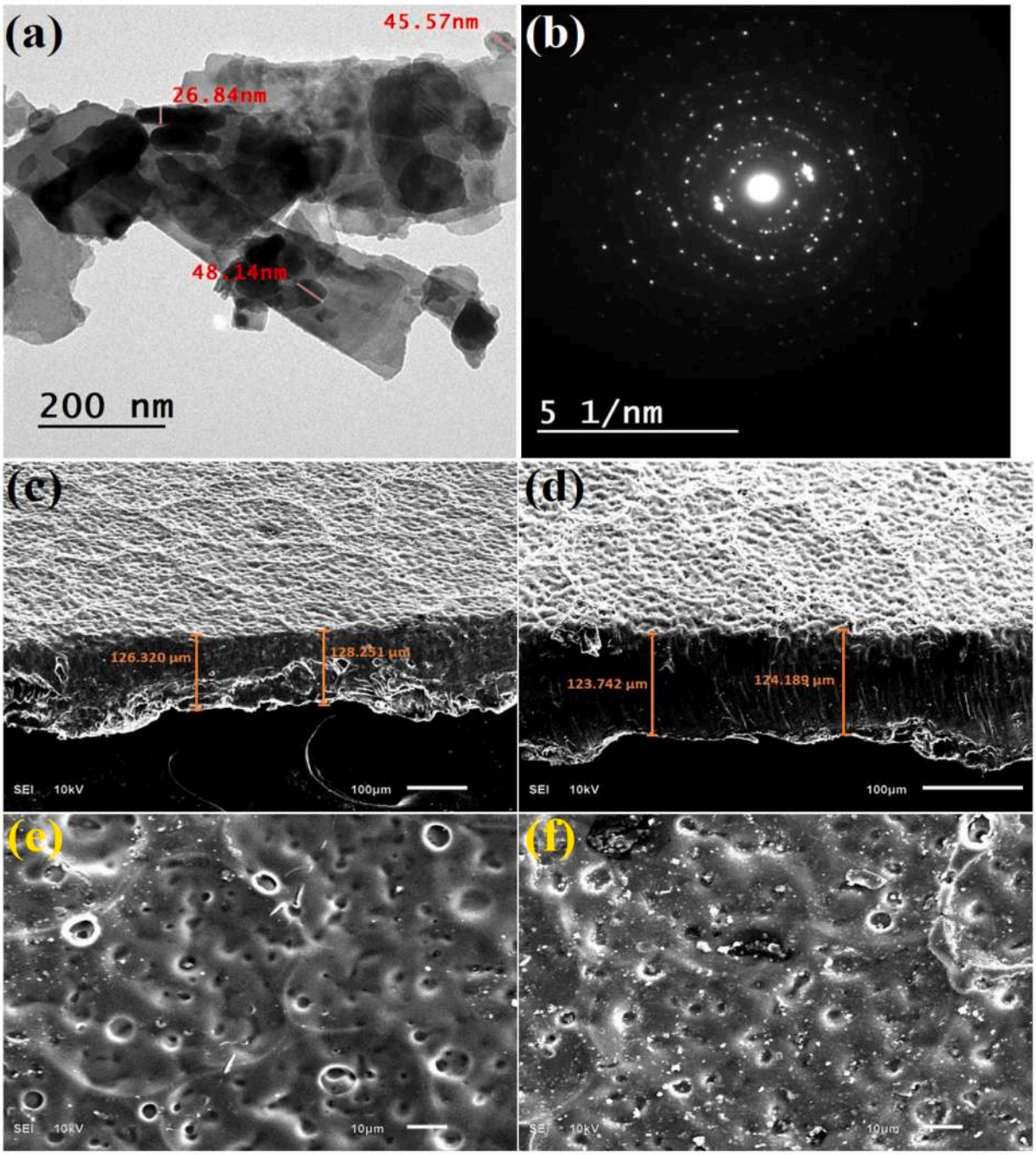

Fig. 2. (a,b) HR-TEM and selected area electron diffraction (SAED) of Bi_2O_3 NC, (c,d) SEM cross-sectional view and (e,f) top view of 1.0 and 6.0 wt% Bi_2O_3 NC/blend films.

maximum (peak) value of PVAc/PVC increased from 3.8×10^{14} s^{-1} to 11×10^{14} s^{-1} at 6.0 wt% Bi_2O_3 NC level. Similarly, incorporating 3.0 wt % Bi_2O_3 NPs increased the $\sigma_{UV/vis}$ of the PVA/PVP blend by about one order of magnitude (Alruwaili & El Sayed, 2024b). These results illustrate the ability of Bi_2O_3 NC to improve the optical parameters of the PVAc/PVC materials.

3.3. TGA and DSC thermal analyses

Fig. 5(a) shows the weight reduction (W%) during the heat treatment in the range of 30–600 °C. No W% during the heating up to 100 °C. All films lose about 6.0 % of their initial weight in the range of 100–220 °C, owing to the evaporation of any residual traces of the THF solvent, moisture, and CO_2 adsorbed on the film surface (The absorption band at 2351 cm^{-1} in the FTIR spectra indicates to the presence of CO_2). The temperature at which the blend starts to decompose (T_o) is 270 °C, and reduced to 223 °C for Bi_2O_3 NC/blend films. The degradation of PCP filled with Bi_2O_3 indicated that the fillers reduced the polymer's thermal stability, and HCl was released at a lower temperature (Messele et al., 2025). Therefore, the films under study are thermally stable up to temperatures in the range of 223–270 °C. The 1st derivative of W% shown in Fig. 5(b) indicates that the main decomposition of the PVAc/PVC blend (dehydrochlorination and molecular weight reduction) occurs at $T_{max} = 301$ °C, which decreased to 299.5, 298, and 290 °C upon loading 1.0, 3.0 and 6.0 wt% Bi_2O_3 NC. One can observe that 3.0 and 6.0 wt% Bi_2O_3 NC-loaded films have a pre-decomposition

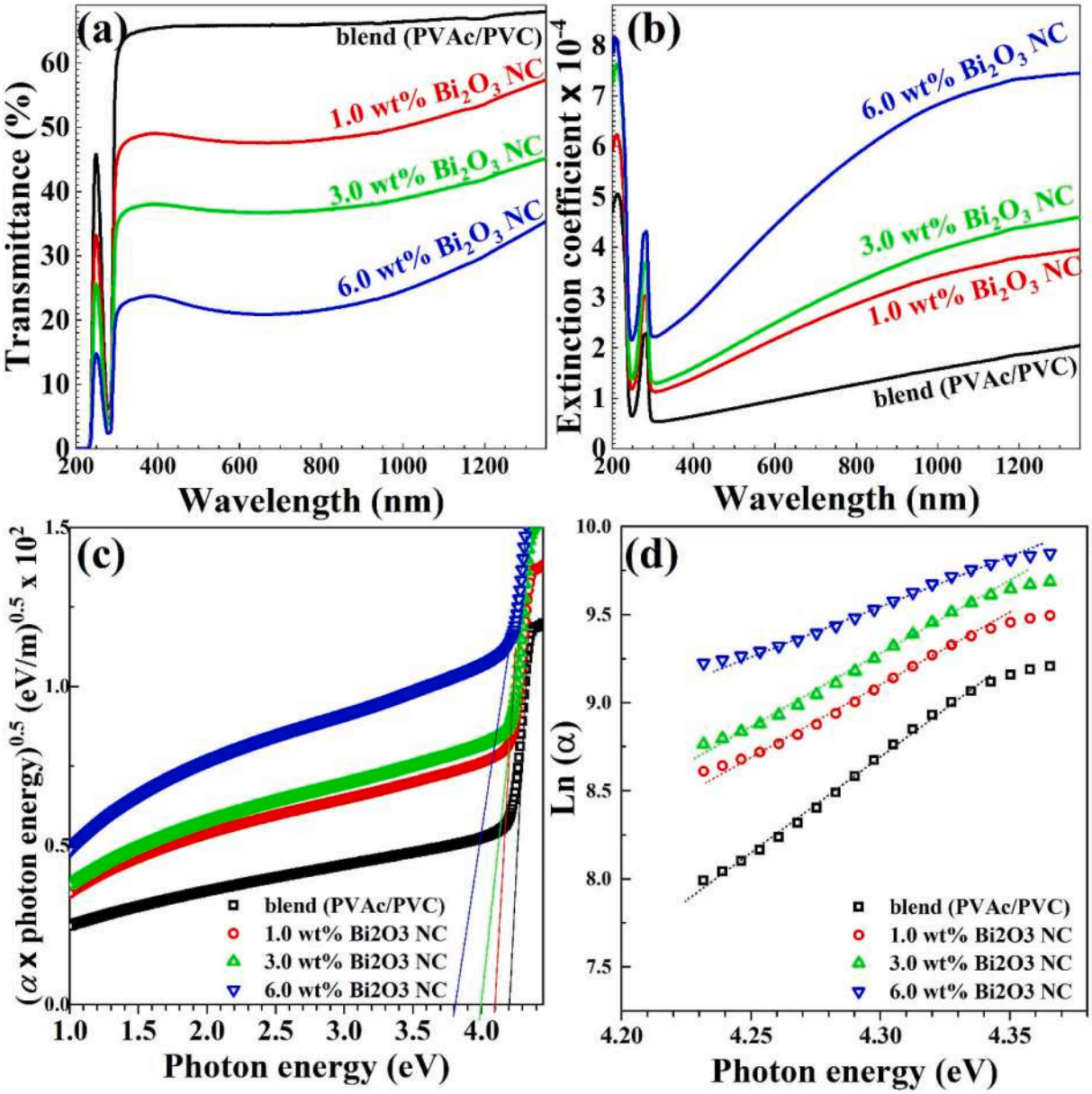

Fig. 3. (a, b) transmittance and extinction coefficient, (c,d) Tauc's plot and Urbach energy determination for Bi_2O_3 NC-doped PVAc/PVC films.

temperature at 240 and 246 °C, respectively. These results mean that the fillers act as catalysts for the blend decomposition (Nancy D'Souza et al., 2020). The remaining weight after the stage is in the range of 30–40 %.

A 2^{ed} decomposition stage is observed in the temperature range 430–520 °C, centered at 450 °C, where the blend's functional groups burn and release CO_2. After this stage, the remaining weight (13–24 %) is a char (carbonaceous residues), and this amount keeps an order regarding the Bi_2O_3 NC load. The phase transitions (glass transition and melting) are interesting phenomenon in polymeric materials, which impacted by the preparation conditions and additives (Alhazime et al., 2019). Fig. 5(c) shows the DSC thermograms of the films. There is an observable one glass transition temperature for each film at about 73.5–75 °C. The curve of the blend shows two endothermic peaks centered around 293 and 470 °C, referring to the melting (T_m) and decomposition (T_d) points, respectively. These points shifted to 291 and 460 °C upon loading at 1.0 wt% Bi_2O_3 NC, then to 245 and 462 °C at 6.0 wt% Bi_2O_3 NC. The presence of a single glass transition/melting temperature confirms good miscibility of PVAc and PVC. These results illustrate the phase transitions of PVAc/PVC thermoplastic blend can be modified by appropriate amounts of Bi_2O_3 NC.

3.4. Radiation shielding

The LAC values were simulated for the prepared composites across the 15–356 keV energy range. The films' LACs showed a high reduction against raising the γ-ray energy across the mentioned interval. The strong reduction is attributed to the photoelectric interaction (PE), which is the main interaction along the energy interval varied between 15 and 100 keV. Along the PE interval, the interacting cross-section (σ) varied inversely with $E_\gamma^{3.5}$ (Muthamma et al., 2020), which means that the small increase in the E_γ values was followed by a strong reduction in the σ. Furthermore, the increment in σ values decreases the number of interactions among the γ-photons and electrons within the atoms of prepared composites. Hence the number of absorbed photons (I_a) decreased within the prepared composites while the transmitted photons (I_t) increased. This increase in the (I_t) with raising the E_γ values leads to a decrease in the (I_o/I_t) ratio and LACs of the prepared composites. Fig. 6 depicts that the increase in E_γ photons from 15 to 100 keV

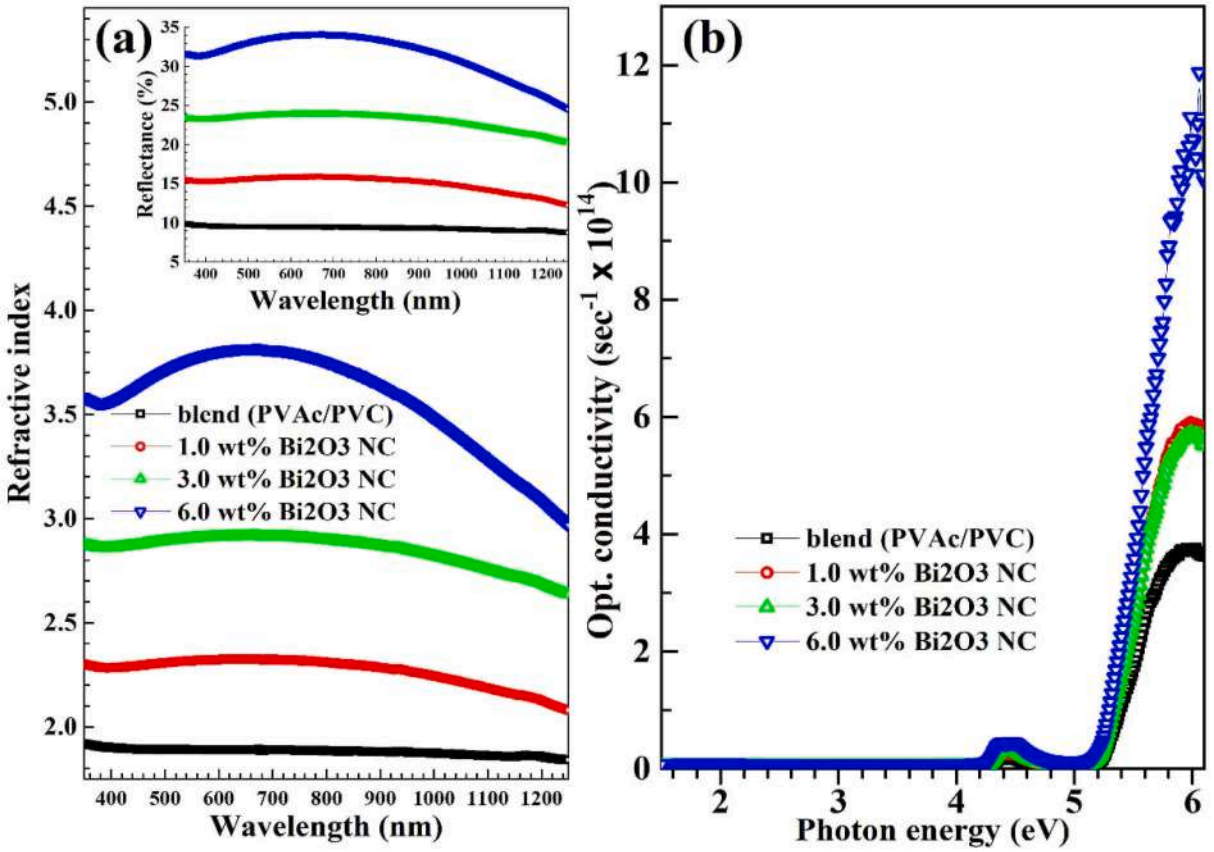

Fig. 4. (a) refractive index (inset shows the reflectance spectra), and (b) optical conductivity of Bi_2O_3 NC-doped PVAc/PVC films.

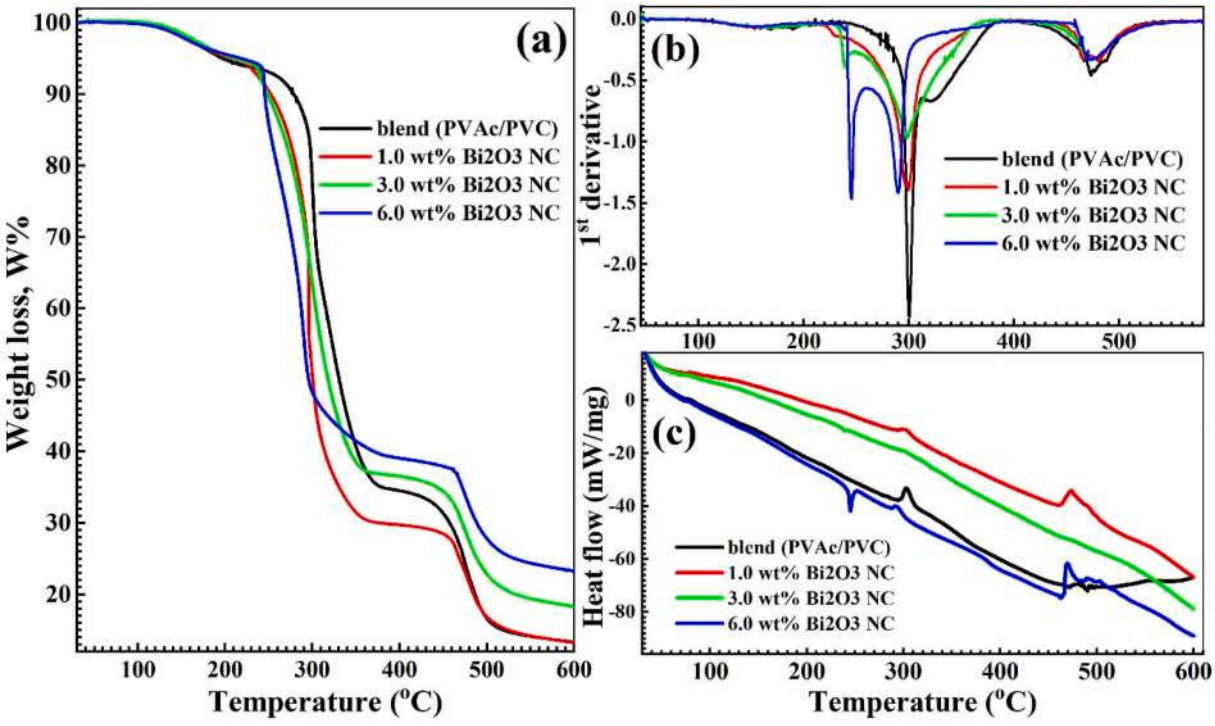

Fig. 5. (a) TGA, (b) 1st derivative, (c) DSC thermograms of Bi_2O_3 NC-doped PVAc/PVC films.

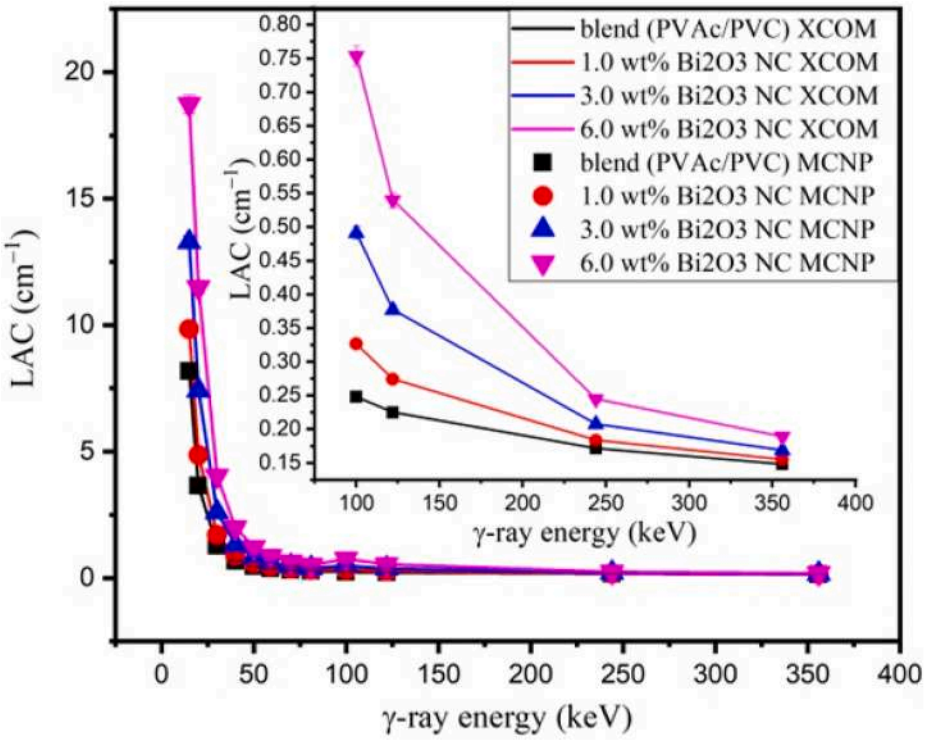

Fig. 6. Variation of the linear attenuation coefficient versus the γ-ray energy (keV).

is accompanied by a decrease in the LACs across the 8.185–0.248 cm^{-1} (for the blend (PVAc/PVC), 9.835–0.326 cm^{-1} (for the 1.0 wt% Bi_2O_3 NC composite), 13.280–0.491 cm^{-1} (for the 3.0 wt% Bi_2O_3 NC composite), and 18.726–0.754 cm^{-1} (for the 6.0 wt% Bi_2O_3 NC composite) ranges. Then the increase in the photon energy from 100 keV to 356 keV, the PE interaction decreased within the prepared composites while the Compton scattering (Cs) increased and became the main interaction within the prepared composites. Since the Cs interaction has σ values

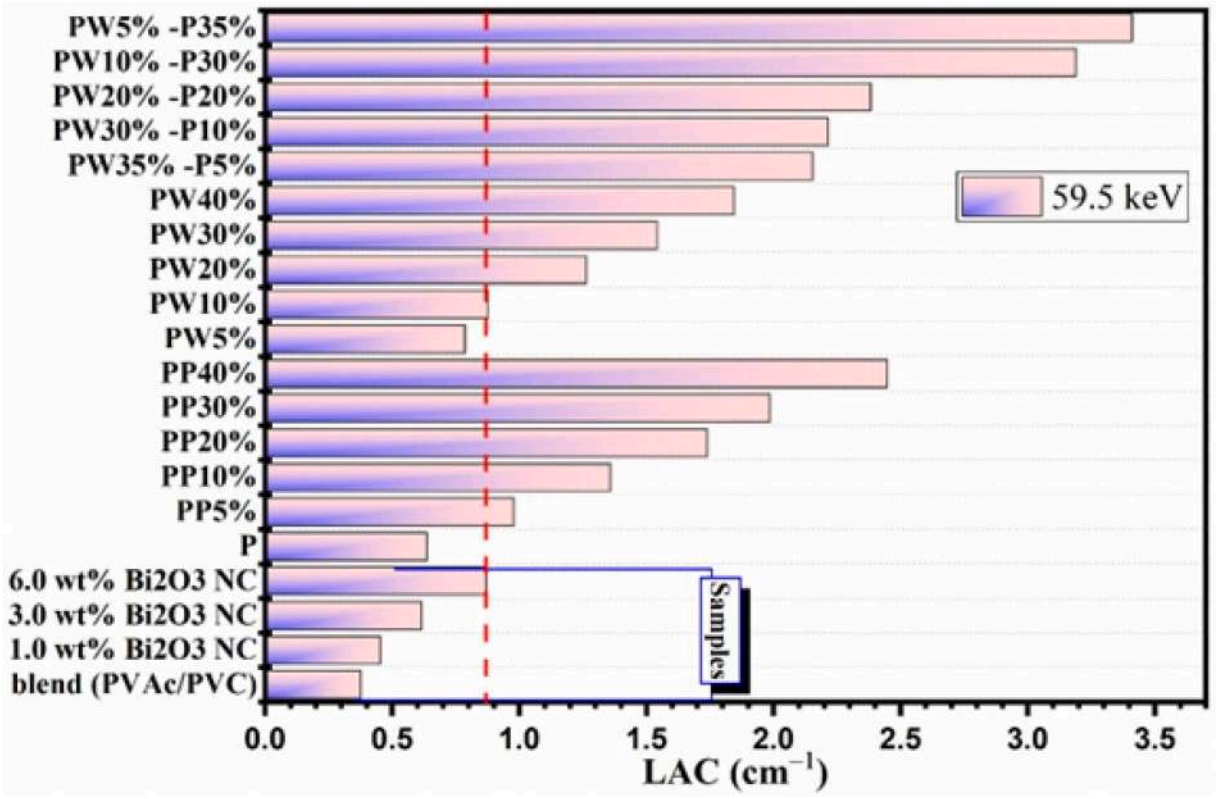

Fig. 7. Comparing the LAC of the fabricated Bi_2O_3 NC/PVAc/PVC composites to the LACs of similar PVC doped PbO and WO_3 compounds selected from the literature.

inversely varied with E_γ (Abdel-Kader & Mohamed, 2024; Mahmoud et al., 2023), the increase in E_γ energy is associated with a moderate reduction in the I_o/I_t ratio and LACs of the prepared composites. Sub-figure 6 shows that the increase in the E_γ values from 100 to 356 keV is accompanied by a reduction in the LACs over the ranges of 0.248–0.148 cm^{-1} (for the blend (PVAc/PVC), 0.326–0.155 cm^{-1} (for the 1.0 wt% Bi_2O_3 NC composite), 0.491–0.169 cm^{-1} (for the 3.0 wt% Bi_2O_3 NC composite), and 0.754–0.189 cm^{-1} (for the 6.0 wt% Bi_2O_3 NC composite).

Fig. 6 shows agreement between the MCNP-5 simulated data and those calculated using the XCOM program across the studied energy interval. The difference between both methods ranges ±2 %.

To validate the protection capacity of prepared Bi_2O_3 NC/PVAc/PVC composites, the LACs of the fabricated Bi_2O_3 NC/PVAc/PVC composites were compared to the LACs of similar selected PVC-doped various compounds including PbO and WO_3 (Yazdani-Darki et al., 2025), as illustrated in Fig. 7. At 59.5 MeV, the LACs of the synthesized composites blend, 1.0 wt% Bi_2O_3 NC, 3.0 wt% Bi_2O_3 NC, and 6.0 wt% Bi_2O_3 NC are 0.377 cm^{-1}, 0.454 cm^{-1}, 0.615 cm^{-1}, and 0.870 cm^{-1}, respectively. The LAC of blend and 1.0 wt% Bi_2O_3 NC composites are lower than the LACs of the other PVC composites selected from literature (Abdel-Kader & Mohamed, 2024). Additionally, the LAC of 3.0 wt% Bi_2O_3 NC is close to the LAC of P composite (0.638 cm^{-1}) while it is lower than the LACs of other PVC-doped PbO and WO_3. The LAC of the 6.0 wt% Bi_2O_3 NC composite is higher than the P composite, while it is close to the LACs of PW5 % (0.787 cm^{-1}) and PW10 % (0.878 cm^{-1}) with WO_3 content of 5 and 10 wt%.

On the other hand, the LAC of 6.0 wt% Bi_2O_3 NC is lower than the LACs of PP5 % (0.979 cm^{-1}), PP10 % (1.359 cm^{-1}), PP20 % (1.740 cm^{-1}), PP30 % (1.986 cm^{-1}), PP40 % (2.448 cm^{-1}), PW20 % (1.263 cm^{-1}), PW30 % (1.543 cm^{-1}), PW40 % (1.844 cm^{-1}), PW35 % -P5 % (2.154 cm^{-1}), PW30 % -P10 % (2.215 cm^{-1}), PW20 % -P20 % (2.382 cm^{-1}), PW10 % -P30 % (3.189 cm^{-1}), and PW5 % -P35 % (3.410 cm^{-1}) (Abdel-Kader & Mohamed, 2024).The high LACs for the selected PP5 %, PP10 %, PP20 %, PP30 %, PP40 %, PW20 %, PW30 %, PW40 %, PW35 % -P5 %, PW30 % -P10 %, PW20 % -P20 %, PW10 % -P30 %, and PW5 % -P35 % composites are attributed to the high content of PbO, WO_3, and a mixture of PbO + WO_3 that varied between 10 and 40 wt%.

The shielding parameters HVL, TEL, TF, and RPE all were calculated based on the simulated MCNP data over the E_γ interval of 15–356 MeV. The impact of variation of the E_γ values on the mentioned shielding parameters was illustrated in Fig. 8(a–d). Due to the reverse relation between LACs and HVLs illustrated in Eq. (2), the reduction in the LACs is accompanied by an increase in the HVLs along the selected E_γ interval. The increase in E_γ values increases the (I_t) photons, which required a thicker HVL to achieve the relation $I_t = 0.5\ I_o$. According to the data presented in Fig. 8(a), the increase in E_γ from 15 keV to 356 keV is followed by an increase in the HVLs throughout the thickness of 0.085–4.678 cm, 0.070–4.475 cm, 0.052–4.113 cm, and 0.037–3.670 cm for the composites blend, 1.0 wt% Bi_2O_3 NC, 3.0 wt% Bi_2O_3 NC, and 6.0 wt% Bi_2O_3 NC, respectively.

It is known that around 0.05 cm of lead equivalent thickness (LET) is required to protect all personnel in a fluoroscopic room. In the current study, the LET was calculated based on the LACs of fabricated composites and the LAC of pure lead. The 0.05 cm lead equivalent was calculated for the prepared composites as illustrated in Fig. 8(b). The increase in E_γ values from 15 keV to 356 keV is associated with a decline in the LET across the thicknesses of 7.704–1.096 cm (for the PVAc/PVC blend, 6.411–1.048 cm (for the 1.0 wt% Bi_2O_3 NC composite), 4.748–0.963 cm (for the 3.0 wt% Bi_2O_3 NC composite), and 3.367–0.859 cm (for the 6.0 wt% Bi_2O_3 NC). This decline in the LETs is attributed to the decline in the LACs of pure lead and the prepared composites. Additionally, over the investigated energy range, increases in the LETs of prepared composites were detected around energies of 30

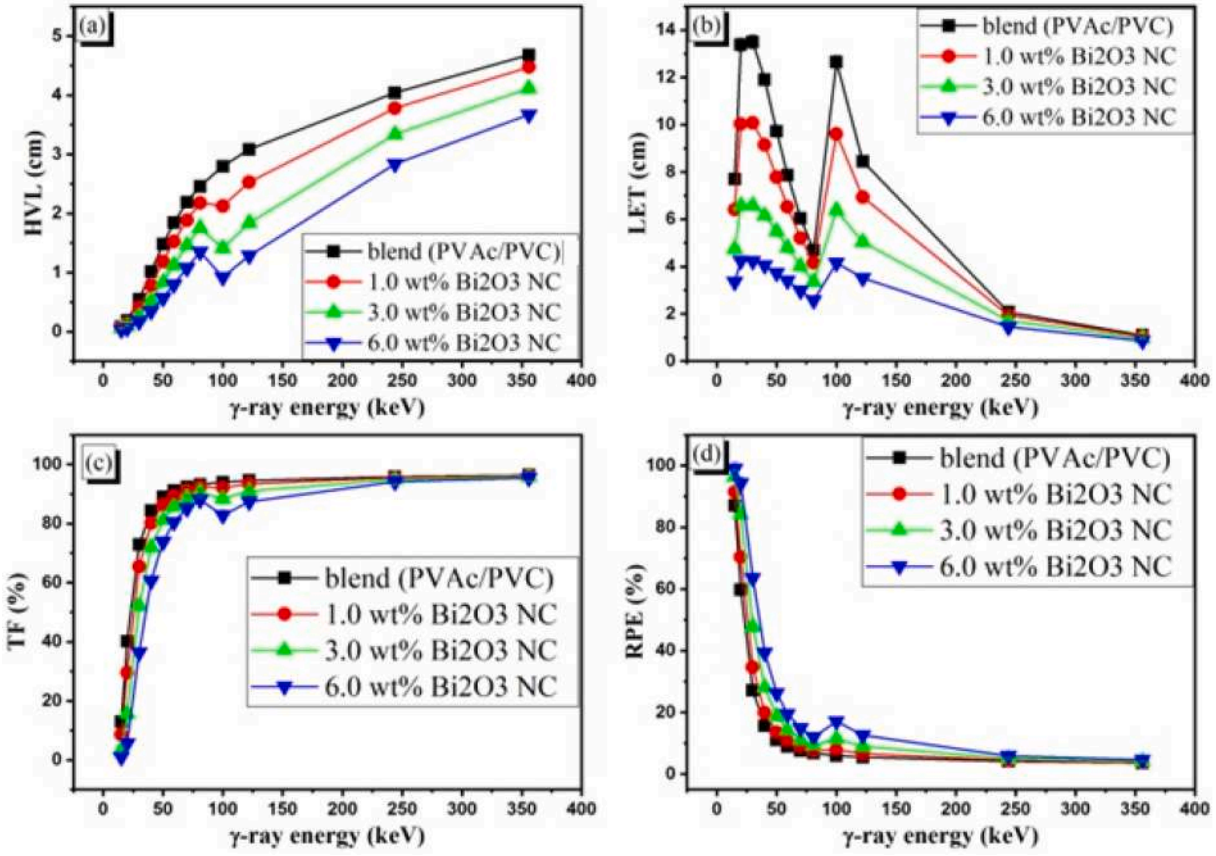

Fig. 8. (a–d): The influence of γ-ray energy on HVL, TEL, TF (%), and RPE (%).

keV and 100 keV, which are attributed to the L1 and K edges of Pb. At L1 and K-absorption edges, the LACs increase to high values, which increases the required LETs, as illustrated in Fig. 8(b).

As previously mentioned, the increase in E_γ values decreases the σ and (I_a) photons, while the (I_t) photons increase. This leads to a significant increase in the (I_t/I_o) ratio and TFs of prepared composites associated with a reduction in the (I_a/I_o) ratio and RPEs when the E_γ increased (see Fig. 8(c) and (d)). The increase in the E_γ from 15 to 356 keV causes a significant increase in the TFs from 12.923 % to 96.364 % (for the blend, from 8.555 % to 96.201 % (for the 1.0 wt% Bi_2O_3 NC composite), from 3.615 % to 95.874 % (for the 3.0 wt% Bi_2O_3 NC composite), and from 0.926 % to 95.388 % (for the 6.0 wt% Bi_2O_3 NC composite), as illustrated in Fig. 8(c). In contrast, Fig. 8(d) shows a reduction in the RPEs of the fabricated composites across the percentages of 87.077–3.636 % (for the blen), 91.445–3.799 % (for the 1.0 wt% Bi_2O_3 NC composite), 96.385–4.126 % (for the 3.0 wt% Bi_2O_3 NC composite), and 99.074–4.612 % (for the 6.0 wt% Bi_2O_3 NC composite) when the E_γ raised from 15 keV to 356 keV, respectively.

The addition of Bi_2O_3 NC concentration to the blend increases the electron density within the prepared composites due to the high atomic number of Bi_2O_3. This increase in the electron density is associated with an increase in the effective atomic number (Z_{eff}) of the prepared composites. According to the data presented in Fig. 9, the increase in Bi_2O_3 NC concentration from 0 wt% to 6 wt% increases the Z_{eff} of the fabricated composites from 11.611 to 30.694. This increase in the Z_{eff} increases the density of the prepared composites, where the ρ of fabricated composites raised from 1.410 g/cm^3 to 1.647 g/cm^3 when the Bi_2O_3 NC concentration raised from 0 wt% to 6 wt%, respectively. The diffusion of the Bi_2O_3 NC within the pores of the blend compound is responsible for the increase in the density of the synthesized composites. This process increases the mass of the fabricated composites without affecting their volume.

The Z_{eff} value also has a great effect on the shielding parameters, especially at low energy, due to the variation of σ with $Z_{eff}^{4.6}$ and Z_{eff} at the PE and Cs intervals (Abbas et al., 2022). As a result, the factors affecting the Z_{eff} values of the synthesized composites also affect the radiation shielding parameters. Therefore, the effect of raising the Bi_2O_3 NC concentration within the synthesized composites was outlined in the next few statements.

Fig. 10(a) reveals an increase in the LACs of the synthesized composites across the intervals of 0.377–0.870 cm^{-1} (at 59 keV), 0.282–0.513 cm^{-1} (at 81 keV), and 0.172–0.244 cm^{-1} (at 244 keV) when the Bi_2O_3 NC content raised from 0 wt% to 6 wt%. The increase in Bi_2O_3 NC increases the Z_{eff} of synthesized composites, which causes an increase in the number of interactions between γ-photons and the electrons within the composite's atoms. This increase in the interaction numbers increases the (I_a) photons, while the (I_t) photons decreased. The clarified decrease in the (I_t) photons increases the (I_o/I_t) ratio and LACs of the synthesized composites. Additionally, the decrease in the (I_t) photons causes a significant decrease in the thickness required to achieve the relation $I_t = 0.5I_o$ (i.e., HVLs of the synthesized composites reduced). Fig. 10(b) depicts that the increase in the Bi_2O_3 NC concentration from 0 wt% to 6 wt% is accompanied by a decline in the HVLs of synthesized composites over the ranges of 1.841–0.796 cm (at 59 keV), 2.458–1.352 cm (at 81 keV), and 4.040–2.836 cm (at 244 keV). Furthermore, the increase in (I_a) photons as the Bi_2O_3 NC content raises the (I_a/I_o) ratio and the RPEs for the synthesized composites, as clarified in Fig. 10(d). The enrichment in the Bi_2O_3 NC concentration from 0 wt% to 6 wt% enhances the RPEs of the synthesized composites across the intervals of 8.984–19.555 % (at 59 keV), 6.808–12.033 % (at 81 keV), and 4.199–5.927 % (at 244 keV), respectively.

The increase in the LACs of the synthesized composites as a result of raising the Bi_2O_3 NC content enhances their shielding capacity compared to the shielding capacity of lead. Fig. 10(c) reveals that the increase in the Bi_2O_3 NC concentration from 0 wt% to 6 wt% decreases the LETs for synthesized composites from 7.864 cm to 3.402 cm (at 59 keV), from 4.700 cm to 2.585 cm (at 81 keV), and from 2.075 cm to 1.456 cm (at 244 keV). The decrease in the LET is a result of the enhancement in the LACs of prepared composites compared to the LACs of Pb as the Bi_2O_3 NC concentration raised within the samples.

4. Conclusions

Bi_2O_3 NC and Bi_2O_3 NC/PVAc/PVC films were prepared by sol-gel and casting techniques. The FTIR spectra revealed improved the interaction of Bi_2O_3 NC/PVAc/PVC films with the surroundings, and the

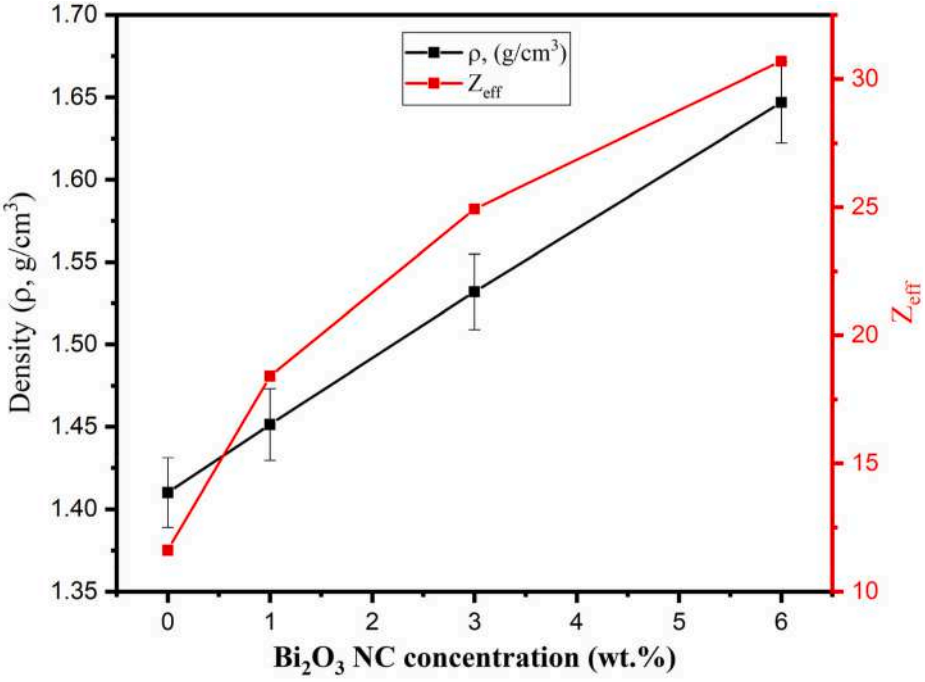

Fig. 9. Impact of Bi_2O_3 NC concentration (wt.%) on the density and Z_{eff} values.

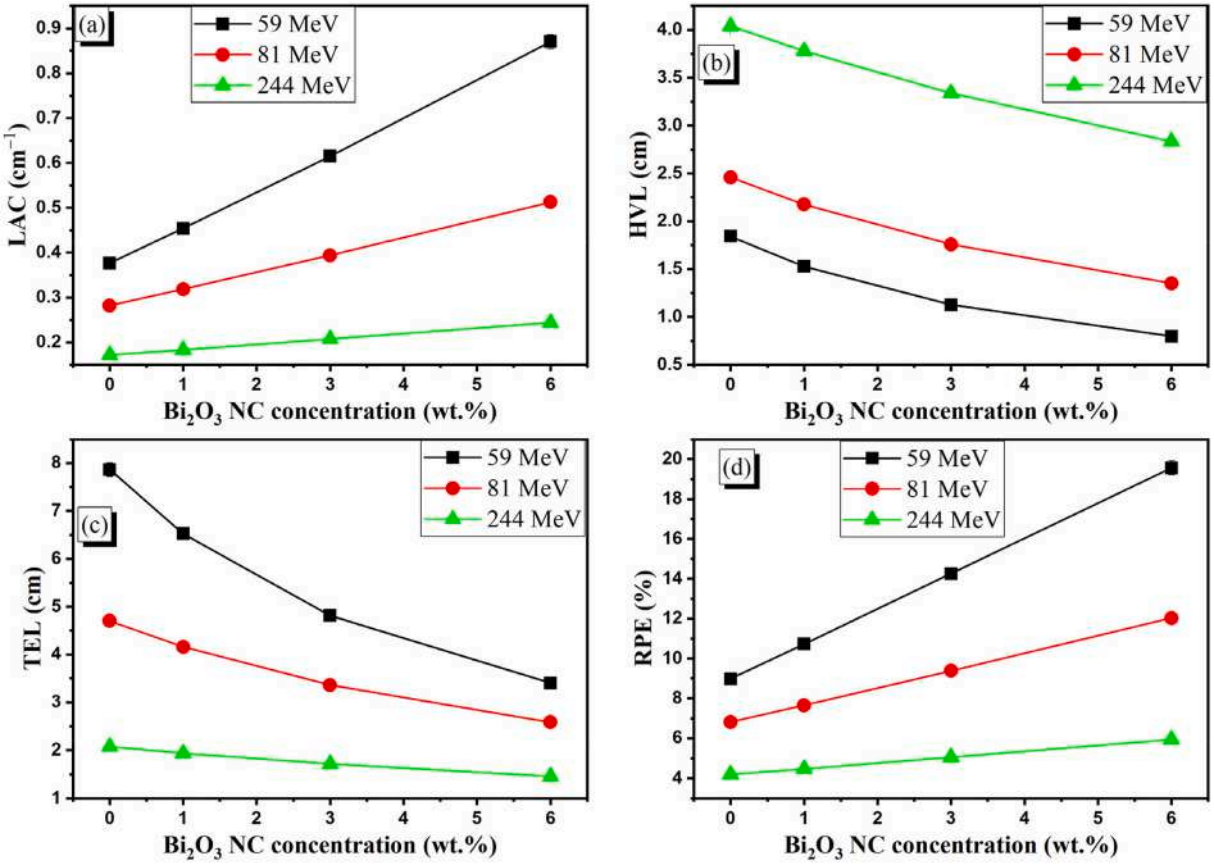

Fig. 10. (a–d)**:** The influence of Bi_2O_3 NC concentration (wt%) on the LAC, HVL, TEL, and RPE (%) radiation shielding parameters.

hydrogen bonding in the composites restricted some vibrations. XRD resulted showed the amorphous nature of the blend, and the incorporation of α-Bi_2O_3 NC of monoclinic structure in the blend. SAED confirmed the good crystallinity of α-Bi_2O_3. SEM images indicated the spongy-like morphology and porous structure of the film surface. The UV–vis transmittance was reduced from 66 to 35 %, and the absorption index of the films was improved with increasing Bi_2O_3 NC level. The films' E_g was reduced from 4.2 to 3.9 eV, and the E_U increased from 88 to 181 meV. The index of refraction significantly increased from 1.9 to about 3.8 with bell-shaped behavior with λ. The films' optical conductivity showed a sudden increase in the UV region and significantly increased with increasing Bi_2O_3 NC content. The films exhibited thermal stability up to 223–270 °C. TGA and DSC thermograms indicated that T_o, T_{max}, T_m, and T_d are strongly dependent on the film composition. According to the Monte Carlo examination for radiation protection properties, the increase of Bi_2O_3 NC concentration from 0 to 6 wt% increases the linear attenuation coefficient of synthesized composites across the ranges of 0.377–0.870 cm^{-1} (at 59 keV), 0.282–0.513 cm^{-1} (at 81 keV), and 0.172–0.244 cm^{-1} (at 244 keV). The increase in the linear attenuation coefficient causes a significant reduction in the lead equivalent thickness for the synthesized composites. The thickness of the fabricated composites equivalent to 0.05 cm of Pb varied throughout 7.864–3.402 cm (at 59 keV), 4.700–2.585 cm (at 81 keV), and 2.075–1.456 cm (at 244 keV) when the Bi_2O_3 NC concentration raised between 0 wt% and 6 wt%. The results that have been discussed indicate that the incorporation of 6 wt% of Bi_2O_3 NC into the synthesized films results in a significant enhancement of the γ-ray protection of the films, which can be utilized for protective purposes during diagnostic and nuclear therapy procedures.

CRediT authorship contribution statement

Mohammad W. Marashdeh: Writing – original draft, Validation, Software, Project administration, Methodology, Funding acquisition, Formal analysis, Data curation. **Aya H. Ahmed:** Writing – original draft, Visualization, Validation, Methodology, Investigation, Formal analysis, Data curation, Conceptualization. **Hanan Akhdar:** Writing – original draft, Visualization, Resources, Project administration, Investigation, Funding acquisition, Conceptualization. **K.A. Mahmoud:** Writing – review & editing, Writing – original draft, Visualization, Validation, Supervision, Software, Project administration, Methodology, Investigation, Formal analysis, Data curation, Conceptualization. **Adel M. El Sayed:** Writing – review & editing, Writing – original draft, Visualization, Validation, Supervision, Software, Methodology, Investigation, Formal analysis, Data curation, Conceptualization. **A. Abou Elfadl:** Writing – review & editing, Writing – original draft, Visualization, Validation, Supervision, Software, Resources, Methodology, Investigation, Formal analysis, Data curation, Conceptualization.

Data availability

Data will be made available on reasonable request.

Conflict of interest

The author declares that there is no conflict of interest reported in this paper.

Acknowledgement

This work supported and funded by the Deanship of Scientific Research at Imam Mohammad Ibn Saud Islamic University (IMSIU)

(grant number IMSIU-DDRSP2503).

Appendix A. Supplementary data

Supplementary data to this article can be found online at https://doi.org/10.1016/j.jrras.2025.101700.

References

Abbas, M. I., El-Khatib, A. M., Dib, M. F., Mustafa, H. E., Sayyed, M. I., & Elsafi, M. (2022). The influence of Bi_2O_3 nanoparticle content on the γ-ray interaction parameters of silicon rubber. *Polymers (Basel), 14*, 1048. https://doi.org/10.3390/polym14051048

Abdel-Kader, M. H., & Mohamed, M. B. (2024). Characterizing of PVA/CMC/MWCNTs nanocomposite films doped Zn0.9Ni0.1S nanoparticles for comprehensive γ-ray radiation shielding performance. *Radiation Physics and Chemistry, 224*, Article 112027. https://doi.org/10.1016/j.radphyschem.2024.112027

Abdelghany, A. M., Meikhail, M. S., & Asker, N. (2019). Synthesis and structural-biological correlation of PVC\PVAc polymer blends. *Journal of Materials Research and Technology, 8*(5), 3908–3916. https://doi.org/10.1016/j.jmrt.2019.06.053

Abou Elfadl, A., Tarek, E., & El Sayed, A. M. (2022). Improving the optical and thermal properties, and stress-strain behavior of a PV(Ac–C) blend using PbO and MgO nanofillers: A comparative study. *Journal of Physics and Chemistry of Solids, 170*, Article 110963. https://doi.org/10.1016/j.jpcs.2022.110963

Ahamed, M., Akhtar, M. J., Khan, M. A. M., Alaizeri, Z. M., & Alhadlaq, H. (2021). Facile synthesis of Zn-doped Bi_2O_3 nanoparticles and their selective cytotoxicity toward cancer cells. *ACS Omega, 6*, 17353–17361. https://doi.org/10.1021/acsomega.1c01467

Alanazi, T. I., & El Sayed, A. M. (2023). Characterization of Mg–Pb–O systems, and MgPbO–thermoplastic blend: Nanocomposites for photonic and microelectronic devices. *Journal of Physics and Chemistry of Solids, 178*, Article 111346. https://doi.org/10.1016/j.jpcs.2023.111346

Alhazime, A. A., Mohamed, M. B., & Abdel-Kader, M. H. (2019). Effect of Zn1−xMgxS doping on structural, thermal and optical properties of PVA. *Journal of Inorganic and Organometallic Polymers and Materials, 29*, 436–443. https://doi.org/10.1007/s10904-018-1014-5

Almuqrin, A. H., Sayyed, M. I., Khandaker, M. U., & Elsafi, M. (2024). Exploring the impact of Bi_2O_3 particle size on the efficacy of dimethylpolysiloxane for medical gamma/X-rays shielding applications. *Radiation Physics and Chemistry, 220*, Article 111629. https://doi.org/10.1016/j.radphyschem.2024.111629

Alruwaili, A., & El Sayed, A. M. (2024a). Boosting the structure, thermal, optical and dielectric properties of a thermoplastic polymer by some nanoperovskites. *Pramāna (Bangalore), 98*, 163. https://doi.org/10.1007/s12043-024-02850-y

Alruwaili, A., & El Sayed, A. M. (2024b). Characterization and the physical properties of nano-sized Bi_2O_3/polymer for energy and high-refractive index applications. *Respiration Physiology, 61*, Article 107746. https://doi.org/10.1016/j.rinp.2024.107746

Alyousef, H. A., Alotiby, M. F., Tijani, S. A., & Alotaibi, B. M. (2023). A study on the use of PMMA - Bi_2O_3 polymer composites as a replacement for concrete and gypsum at diagnostic photon energies. *Journal Rad Research Application Science, 16*, Article 100707. https://doi.org/10.1016/j.jrras.2023.100707

Dogan, M., Turan, M., Beyli, P. T., Bicil, Z., & Kizilduman, B. K. (2021). Thermal and kinetic properties of poly(vinylacetate)/modified MWCNT nanocomposites. *Fullerenes, Nanotubes, and Carbon Nanostructures, 29*(6), 475–485. https://doi.org/10.1080/1536383X.2020.1860945

Echeweozo, E. O., Kırkbınar, M., Alomairy, S., & Al-Buriahi, M. S. (2025). Gamma radiation and charged particle shielding properties of Polymethyl methacrylate-Bi_2O_3 composite for medical shielding applications: Synthesis and simulation study. *Journal Rad Research Application Science, 18*, Article 101247. https://doi.org/10.1016/j.jrras.2024.101247

El Sayed, A. M., Abdelghany, A. M., & Abou Elfadl, A. (2022). Structural, optical, mechanical and antibacterial properties of MgO/poly(vinyl acetate)/poly(vinyl chloride) nanocomposites. *Brazilian Journal of Physics, 52*, 150. https://doi.org/10.1007/s13538-022-01156-x

El Sayed, A. M., & Mohamed, A. D. M. (2018). Synthesis, structural, thermal, optical and dielectric properties of chitosan biopolymer; influence of PVP and α-Fe_2O_3 nanorods. *Journal of Polymer Research, 25*, 175. https://doi.org/10.1007/s10965-018-1571-x

El Sayed, A. M., & Morsi, W. M. (2013). Dielectric relaxation and optical properties of polyvinyl chloride/lead monoxide nanocomposites. *Polym. Comps., 34*(12), 2031. https://doi.org/10.1002/pc.22611

Elashwai, I. S., Hakeem, N. A., & Abdelrazek, E. M. (2008). Spectroscopic and thermal studies of PS/PVAc blends. *Physica B, 403*, 3547–3552. https://doi.org/10.1016/j.physb.2008.05.024

Gholamzadeh, L., & Mehrjardi, A. Z. (2024). Bismuth (III) oxide (Bi_2O_3)/poly (vinyl alcohol) nanocomposite fiber-coated polyester fabrics for multifunctional applications. *Clean Technologies and Environmental Policy, 26*, 3859–3868. https://doi.org/10.1007/s10098-023-02533-z

Ghule, P. G., Bholane, G. T., Joshi, R. P., Dahiwale, S. S., Shelke, P. N., & Dhole, S. D. (2024). Gamma radiation shielding properties of unsaturated polyester/Bi_2O_3 composites: An experimental, theoretical and simulation approach. *Radiation Physics and Chemistry, 216*, Article 111452. https://doi.org/10.1016/j.radphyschem.2023.111452

Hamisu, A., Khiter, O., Al-Zhrani, S., Haridh, W. S. B., Al-Hadeethi, Y., Sayyed, M. I., & Tijani, S. A. (2024). The use of nanomaterial polymeric materials as ionizing radiation shields. *Radiation Physics and Chemistry, 216*, Article 111448. https://doi.org/10.1016/j.radphyschem.2023.111448

Kamaruddin, K. E., Kok, S. Y., Ramli, R. M., & Azman, N. Z. N. (2024). X-ray attenuation measurement of electrospun polymer composite mats containing Bi_2O_3/WO_3 nanofillers as X-ray shielding material. *Applied Physics A, 130*, 455. https://doi.org/10.1007/s00339-024-07600-w

Kassim, H., Asemi, N. N., & Aldawood, S. (2025). Gamma-ray shielding enhancement using glycidyl methacrylate polymer composites reinforced by titanium alloy and bismuth oxide nanoparticles. *Journal Rad Research Application Science, 18*, Article 101202. https://doi.org/10.1016/j.jrras.2024.101202

Kavgacı, M., & Eskalen, H. (2023). Morphology, structure and optical properties of PVA nanocomposites reinforced with bismuth oxide nanoparticles and carbon quantum dots. *Journal of Materials Science: Materials in Electronics, 34*, 1229. https://doi.org/10.1007/s10854-023-10617-1

Khan, H. U., Jan, M. T., Iqbal, M., Shah, M., Ullah, I., Khan, J., Mahmood, K., Niaz, A., & Tariq, M. (2020). Synthesis, characterization and electrical conductivity of silver doped polyvinyl acetate/graphene nanocomposites: A novel humidity sensor. *Zeitschrift fuer Physikalische Chemie, 234*(1), 27–43. https://doi.org/10.1515/zpch-2018-1302

Koyuncu, B., Aral, N., Candan, C., & Nergis, B. (2024). Bismuth oxide nanoparticles/waterborne polyurethane-coated fabrics for ionizing radiation protection. *Journal of Coatings Technology and Research, 21*(3), 969–978. https://doi.org/10.1007/s11998-023-00864-6

Lakhwani, O. P., Dalal, V., Jindal, M., & Nagala, A. (2019). Radiation protection and standardization. *Journal Clinical Orthoplogy Trauma, 10*(4), 738–743. https://doi.org/10.1016/j.jcot.2018.08.010

Mahmoud, K. A., Tashlykov, O. L., Kropachev, Y., Samburov, A., Zakharova, P., & Abu El-Soad, A. M. (2023). A close look for the γ-ray attenuation capacity and equivalent dose rate form composites based epoxy resin: An experimental study. *Radiation Physics and Chemistry*. , Article 111063. https://doi.org/10.1016/j.radphyschem.2023.111063

Menon, N. H., Sabu, A., & Ramanujam, B. T. S. (2022). Polyvinylidene fluoride-poly (vinyl acetate)-natural graphite blend nanocomposites: Investigations of electroactive phase formation, electrical, thermal, and wetting properties. *Polymers for Advanced Technologies, 33*, 4023–4040. https://doi.org/10.1002/pat.5833

Messele, A. G., Penev, K. I., Mequanint, K., & Mekonnen, T. H. (2025). Lead-free single and dual-filler loaded polychloroprene X-ray shielding nanocomposites. *Applied Materials Today, 42*, Article 102558. https://doi.org/10.1016/j.apmt.2024.102558

Muthamma, M. V., Bubbly, S. G., & Gudennavar, S. B. (2020). Attenuation properties of epoxy-Ta_2O_5 and epoxy-Ta_2O_5-Bi_2O_3 composites at γ-ray energies 59.54 and 662 keV. *Journal of Applied Polymer Science, 137*, 1–12. https://doi.org/10.1002/app.49366

Nancy D'Souza, A., Prabhu, N. S., Sharmila, K., I Sayyed, M., M Somshekarappa, H., Lakshminarayana, G., Mandal, S., & Kamath, S. D. (2020). Role of Bi2O3 in altering the structural, optical, mechanical, radiation shielding and thermoluminescence properties of heavy metal oxide borosilicate glasses. *Journal of Non-crystalline Solids, 542*, Article 120136. https://doi.org/10.1016/j.jnoncrysol.2020.120136

Nunez-Briones, A. G., Benavides, R., Bolaina-Lorenzo, E. D., Martínez-Pardo, M. E., Kotzian-Pereira-Benavides, C., Puente-Urbina, B. A., & García-Cerda, L. A. (2024). Effect of Bi_2O_3 nanostructures on X-ray shielding, thermal, mechanical and biological properties of PVC polymer nanocomposites. *Radiation Physics and Chemistry, 216*, Article 111455. https://doi.org/10.1016/j.radphyschem.2023.111455

Özdemir, E. T., Ertekin, Z., Kara, S., Erol, M., & Seçmen, M. (2024). Enhancing electromagnetic interference shielding performance of polyester fabrics through composite polymer coating with metal oxides and expanded graphite. *Journal of Materials Science: Materials in Electronics, 35*, 1711. https://doi.org/10.1007/s10854-024-13480-w

Sameela, T. P., Sathian, R., Meera, K., Verma, M., & Ramesan, M. T. (2023). Synthesis, characterization and mechanical properties of poly (vinyl acetate)/boehmite nanocomposites via emulsion polymerization. *Journal of Inorganic and Organometallic Polymers and Materials, 33*, 1415–1426. https://doi.org/10.1007/s10904-023-02606-y

Tan, N., Weng, Y., Li, H., Chen, B., Zhao, L., Huang, B., Lu, B., & Tang, L. (2025). Copper abietate/polyvinyl acetate composite film for enhanced humidity sensing in Chinese herbal medicine monitoring systems. *Sensors and Actuators B, 422*, Article 136656. https://doi.org/10.1016/j.snb.2024.136656

Wu, H., Hua, X., Hu, J., Liu, X., & Zhang, J. (2025). Fabrication of stereocomplex-type poly(lactic acid) nanocomposites based on the selective nucleation of poly(vinyl acetate) modified cellulose nanocrystals. *Carbohydrate Polymers, 347*, Article 122716. https://doi.org/10.1016/j.carbpol.2024.122716

X-5 Monte Carlo Team. (2003). *MCNP — a general Monte Carlo N-particle transport code, version 5, La-Ur-03-1987 II*.

Yassene, A. A. M., Abd Elwahab, N. R., & Eyssa, H. M. (2024). Development of HDPE/natural fiberboard nanocomposite reinforced Bi_2O_3/BaO and H_3BO_3: A sustainable approach for gamma and neutron shielding application. *Polymer Engineering & Science, 64*, 3271–3288. https://doi.org/10.1002/pen.26768

Yazdani-Darki, S., Eslami-Kalantari, M., Zare, H., & Ramazani-MoghaddamArani, A. (2025). Preparation and structural characterization of PbO and WO_3-PVC hybrid

nanocomposites for gamma-ray radiation shielding. *Radiation Physics and Chemistry, 229*, Article 112489. https://doi.org/10.1016/j.radphyschem.2024.112489

Yu, X., Xu, Z., Lu, Y., Yang, L., Sun, S., Du, M., Zuo, M., & Zheng, Q. (2025). Effects of selective distribution of poly(methyl methacrylate)-grafted graphene oxide on the phase behavior and conductivity of poly(methyl methacrylate)/poly(vinyl acetate) blends. *Compos. A, 188*, Article 108563. https://doi.org/10.1016/j.compositesa.2024.108563

Zhang, H., Zhu, H., Xu, C., Li, Y., Liu, Q., Wang, S., & Yan, S. (2022). Effect of nanoparticle size on the mechanical properties of polymer nanocomposites. *Polymer, 252*, Article 124944. https://doi.org/10.1016/j.polymer.2022.124944